Available online at www.sciencedirect.com

ScienceDirect

Ceramics International 40 (2014) 1513–1518

CERAMICS INTERNATIONAL

www.elsevier.com/locate/ceramint

Fabrication of anode-supported tubular $Ba(Zr_{0.1}Ce_{0.7}Y_{0.2})O_{3-\delta}$ cell for intermediate temperature solid oxide fuel cells

Sung Hwan Min[a,b], Rak-Hyun Song[d], Jin Goo Lee[a,b], Myoung-Geun Park[a,b], Kwang Hyun Ryu[c], Yu-Kwon Jeon[a,b], Yong-gun Shul[a,b,*]

[a]Department of Chemical and Biomolecular Engineering, Yonsei University, Seoul 120-749, Republic of Korea
[b]The Specialized Graduate School of Hydrogen and Fuel Cell, Yonsei University, Seoul 120-749, Republic of Korea
[c]ENChem. Ltd., Jeongbalsan 1119, Ilsan, Goyang, Gyeonggi 410-828, Republic of Korea
[d]Fuel Cell Research Center, Korea Institute of Energy Research (KIER), 152 Gajeong-ro, Yuseong-gu, Daejeon 305-343, Republic of Korea

Received 1 July 2013; received in revised form 5 July 2013; accepted 5 July 2013
Available online 11 July 2013

Abstract

The characteristics and performance of the anode-supported tubular cells with thin and dense $Ba(Zr_{0.1}Ce_{0.7}Y_{0.2})O_{3-\delta}$ (BZCY) electrolyte was investigated. The fine BZCY powder was prepared by a co-precipitation method. The Ni–BZCY anode tube was fabricated by an extrusion process. Ni–BZCY/BZCY nanocomposite slurry was coated on the anode tube as an anode fuctional layer (AFL) by using the dip-coating method. The BZCY electrolyte and LSCF–BZCY cathode was coated by vacuum slurry coating and dip-coating method, respectively. The anode tube had 0.381 μm in pore size (porosity: 34%). The impedance analysis of the tubular BZCY cells was conducted under open circuit condition. The ohmic resistance and the polarization resistance of the BZCY electrolyte were about 0.78 Ω cm^2 and 0.035 Ω cm^2 at 700 °C, respectively. The performance was measured under humidified H_2 (5% H_2O) atmosphere at 600–700 °C. The maximum power density of the tubular BZCY cell was about 0.5 Wcm^{-2} at 700 °C.

Keywords: Solid oxide fuel cells; BZCY; Functional layer; Proton conductor; Tubular-type

1. Introduction

Fuel cells are simple electrochemical devices that convert chemical energy into electrical energy directly. In particular, a solid oxide fuel cell (SOFC) has received remarkable attention due to high efficiency (including heat energy), low pollutions and fuel flexibility (natural gas and biogas) [1,2]. Despite these advantages, the high operating temperature (about 800–1000 °C) has caused various problems such as increase in the cost of interconnect materials and shortened lifetime of fuel cell system. In order to overcome these problems, significant efforts has been concentrated on reducing operating temperature down to intermediate temperature of 500–700 °C [3].

An electrolyte material is important to reduce operating temperature. A high ionic conductivity has to be needed for the electrolyte materials without electronic conductivity. Doped-zirconia, doped ceria and perovskite-type have been mainly studied as the electrolyte materials. In particular, yttria-stabilized zirconia (YSZ) has been developed as an electrolyte of conventional SOFCs. It shows high ionic conductivity only at high temperature (about 1000 °C) [4]. Samarium or gadolinium doped ceria (SDC or GDC) has also been promising electrolyte materials for intermediate temperature solid oxide fuel cells (IT-SOFCs), but electronic conductivity can appear in reducing atmosphere [5]. These electrolyte materials follow oxygen-ion transport mechanism. On the other hand, a perovskite-type proton conducting materials can enable a proton (H^+) to pass through an electrolyte. Since a proton conduction has lower activation energy than an oxygen ion conduction, it can be easy to reduce the operating temperature

*Corresponding author at: Department of Chemical and Biomolecular Engineering, Yonsei University, Seoul 120-749, Republic of Korea.
Tel.: +82 02 2123 2758; fax: +82 02 312 6507.
E-mail address: shulyg@yonsei.ac.kr (Y.-g. Shul).

0272-8842/$ - see front matter © 2013 Elsevier Ltd and Techna Group S.r.l. All rights reserved.
http://dx.doi.org/10.1016/j.ceramint.2013.07.036

into intermediate temperature [6,7]. In addition, the fuel efficiency can be increased because water vapor as a product is formed at the cathode side. $Ba(Zr_{0.1}Ce_{0.7}Y_{0.2})O_{3-\delta}$ is one of the most promising materials for proton conducting electrolyte materials. BZCY has been reported to exhibit high protonic conduction and sufficient chemical and thermal stability under wide range of operating temperatures [7].

The SOFC system is generally classified as two types of configurations: planar type and tubular type. Not only can planar-type SOFCs be fabricated with ease but it also offers higher power density than the tubular-type cell because electric current path of the tube is increased by the geometrical property of the tubular cell, causing ohmic losses [8,9]. However, in the planar cell, high thickness of anode and cathode parts for a mechanical stability results in high cost of raw ceramic materials. Tubular type SOFCs are more suitable for a large scale than planar type because it can obtain simple seal requirements and a good mechanical property [10]. The various methods such as slip casting [11] and paste extrusion [12] can be used to fabricate a tubular support. The paste extrusion method, in particular, has various advantages to rapidly fabricate a tubular anode support with an uniform density distribution and very complicated cross-sections [13].

In this study, the BZCY material was applied to a tubular-type cell for a large scale. The tubular cells with the configuration of Ni–BZCY/BZCY/LSCF–BZCY was evaluated on the performance and the impedance characteristics. The crystallite structure, porosity, and pore size of the anode were measured using the anode tube fabricated by a paste extrusion method. The BZCY electrolyte was coated by vaccum-assisted dip coating method, and its microstructures and electrical properties were investigated.

2. Experimental

2.1. BZCY power preparation

The $Ba(Zr_{0.1}Ce_{0.7}Y_{0.2})O_{3-\delta}$ nanopowder was prepared by the co-precipitation method. The stoichiometric amount of Ba $(NO_3)_2$ (Yakuri Pure Chemical Co. 99%), $ZrO(NO_3)_2 \cdot H_2O$ (Aldrich, 99%), $Ce(NO_3)_3 \cdot 6H_2O$ (Aldrich, 99%) and Y $(NO_3)_3 \cdot 6H_2O$ (Aldrich, 99.8%) was dissolved in distilled water to form an aqueous solution. Ammonium carbonate ($(NH_4)_2CO_3$) (Aldrich, 99%) was used as a precipitant. The solution with the precursors was dropped very slowly into the ammonium carbonate solution under vigorous stirring at room temperature. The suspension was stirred for 2 h and aged for 6 h at room temperature. The precipitate was washed several times with distilled water (2 times) and ethanols (1 time) until impurities were removed. The clean precipitate was dried at 100 °C for 24 h, and then calcined at 1000 °C for 2 h in air condition. The calcined BZCY powder was ball-milled with zirconia ball in ethanol for 24 h.

2.2. Nanocomposite powder preparation

The NiO/BZCY–BZCY nanocomposite powder was synthesized by a modified Pechini method [14]. The starting salts were $Ni(NO_3)_2 \cdot 6H_2O$ (Junsei Chemical Co., 97% and metal nitrates (Ba, Zr, Ce and Y). The precursors were dissolved in distilled water, and then the citric acid was added into the solution with the precursors. The solution was heated and stirred at 60 °C for 2 h. Ethylene glycol (EG) (Aldrich, 99%) was added to the solution as a polymerization agent. Next, BZCY powder prepared by the co-precipitation method was added to the aqueous solution. The polymeric solution was fired at 240 °C for 4 h. The powder obtained through the firing process was calcined at 1000 °C for 3 h.

2.3. Tubular cell fabrication

The cell configuration of the tubular BZCY cell is shown in Fig. 1. NiO (J.T. Baker Co.) and BZCY powder were mixed with 10 wt% activated carbon as a pore former (NiO: BZCY = 6:4) by the ball-milling method. The anode powder was dried at 100 °C for 24 h. The dried powder was subsequently mixed with an organic binder and distilled water to form a well dispersed paste. The homogenous dispersed paste was pre-extruded to remove moisture using vacuum pump. The paste with less moisture was then extruded to make a tubular anode substrate. The anode tubes were dried by roll milling for about 2–3 days at room temperature, and pre-sintered at 1100 °C for 3 h. The anode functional layer (AFL) was dip-coated on the pre-sintered anode tube. The anode tube with AFL was sintered at 1200 °C for 3 h. The BZCY electrolyte layer was coated on the tube by a vacuum slurry coating method, and then slowly co-sintered at 1450 °C for 5 h. The cathode slurry was prepared using $La_{0.6}Sr_{0.4}Co_{0.2}Fe_{0.8}O_3$ (LSCF, Praxair) and BZCY, and coated by dip-coating

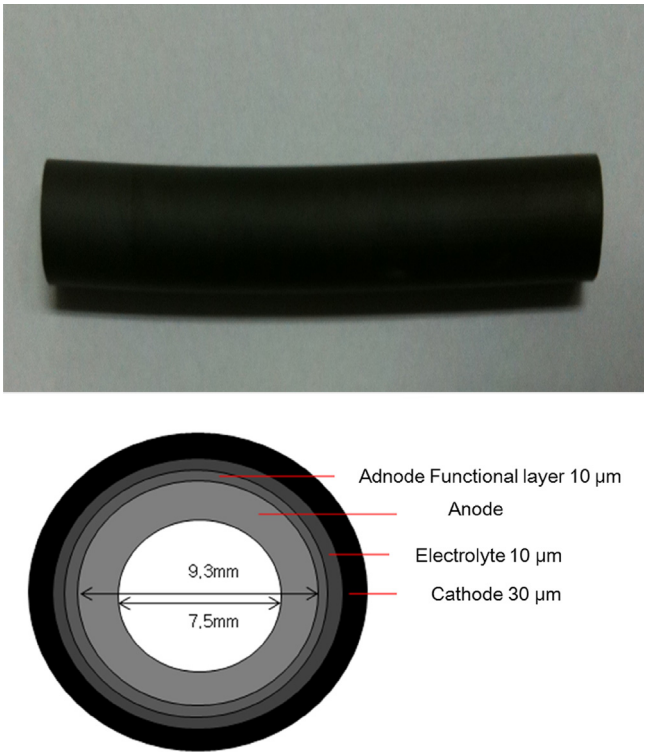

Fig. 1. Cell configuration of the tubular BZCY cell in this study.

process on the tube, which was about 2.07 cm^2 of an active area. The single cell was sintered at 1100 °C for 3 h. In order to secure a sufficient fluidity at the brazing temperature, the design of brazing cap was conducted. The induction brazing was carried out in air atmosphere after assembling the anode-supported tubular cell with the brazing cap.

2.4. Characterization

The crystallite structures of the synthesized powders were detected by an x-ray diffractometer (Rigaku Miniflex). The scanning electron microscopy (SEM) was used to observe the cross-sectional morphologies and the thickness of each layer of the tubular cell. The porosity and pore size of the anode tube were determined by mercury porosimetry (Model Autopore II, Micrometrics Instrument Co.). The impedance of the tubular cells was measured by impedance analyzer (solatron SI 1287 and SI 1260) at open circuit condition. The frequency range was 0.1 Hz–0.1 MHz with amplitude of 10 mV. The cell performance was also tested by solatron equipments. The test was conducted at various temperatures (600–700 °C), and H_2 gas (5% H_2O) was used as a fuel.

3. Results and discussion

Fig. 2 shows X-ray diffraction patterns of the Ba$(Zr_{0.1}Ce_{0.7}Y_{0.2})O_{3-\delta}$ powder synthesized by the co-precipitation method and the anode fuctional layer powder after the calcination process at 1000 °C. The BZCY powder was found to be well-developed crystallization in Fig. 2(a). The peaks of the calcined BZCY powder showed a simple cubic perovskite structure without any secondary phases. The crystallite size of the calcined BZCY powder and the NiO–BZCY powder for anode functional layer were calculated using the Debye Scherrer equation:

$$D = 0.9\lambda / B\cos\theta_B$$

wherein D is the crystallite size, λ is the X-ray wavelength (1.5406 Å), B is the full-width at half-maximum of the corresponding XRD peak and θ_B is Bragg′s angle. The crystallite size of the calcined BZCY powder was 61.7 nm. The crystallite size of the NiO–BZCY anode functional layer powder was 48.5 nm. The BZCY powder by co-precipitation method had larger crystallite size than the AFL powder by the Pechini method.

Fig. 3 shows the porosity of the NiO–BZCY anode tube sintered at various temperatures before and after reduction. The porosity of the anode tube decreased with an increase in sintering temperature because of the intrinsic property of ceramic materials so-called shrinking. The porosity of the anode tube sintered at 1450 °C was about 27% before reduction, but it reached to about 34% after reduction. This may be due to the volume change caused by the conversion of nickel oxide to metallic nickel. Accordingly, the NiO–BZCY anode was considered to obtain sufficient porosity for lower

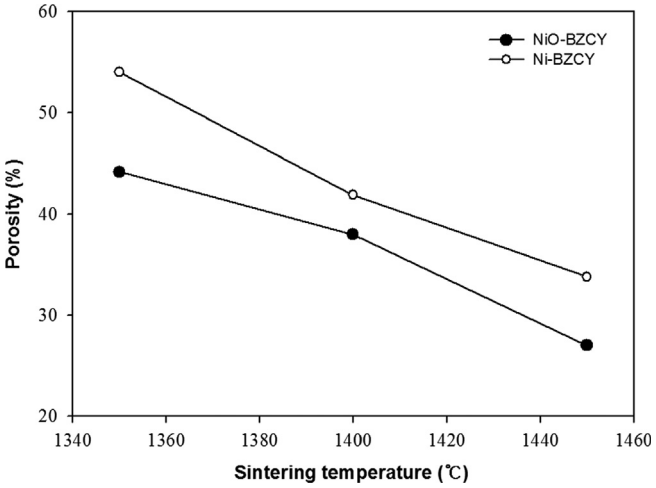

Fig. 3. The porosity of the NiO–BZCY anode tube sintered at various temperatures before and after a reduction.

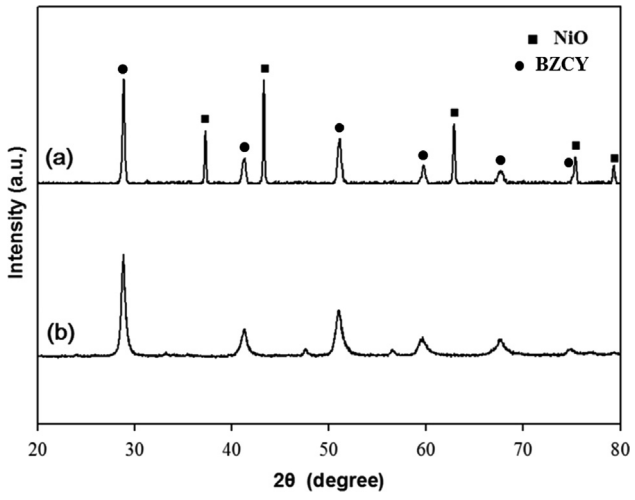

Fig. 2. X-ray diffraction patterns of (a) the BZCY powder and (b) the NiO–BZCY anode functional layer powder calcined at 1000 °C.

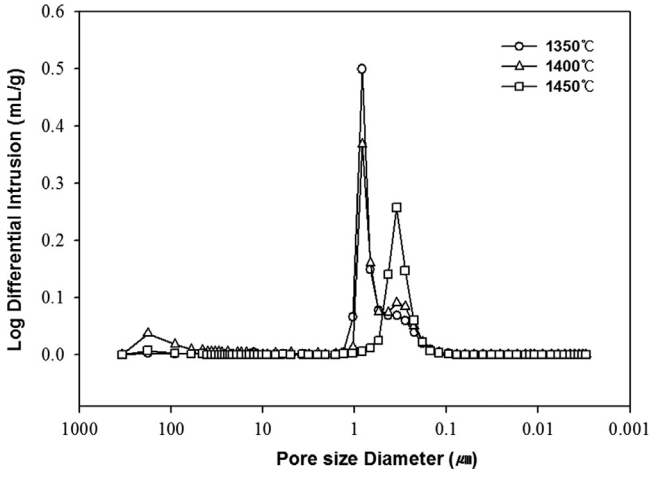

Fig. 4. Pore-size distributions of the tubular NiO–BZCY anode substrate sintered at different temperatures.

concentration polarization even when co-sintered with the BZCY electrolyte at 1450 °C. The pore size distribution of the tubular Ni–BZCY anode is showed in Fig. 4. The average pore diameter of the Ni–BZCY tube sintered at 1450 °C was about 0.38 μm, which is suitable for the SOFC anode. The pore size distribution showed the very narrow monomodal distribution, indicating a uniform pore structure can be obtained in the tubular Ni–BZCY anode. The uniform pore structure can have a positive influence on the increase in the triple phase boundary sites (TPB).

The cross-sectional SEM images of the tubular BZCY cell are shown in Fig. 5. The electrolyte coated by vacuum assisted dip-coating method was sufficiently dense. The interface between the electrodes and electrolyte was well-bonded as Son et al. reported that the electrolyte particles in the slurry can fill up defects on the surface of the anode tube by vacuum slurry coating [15]. The thickness of the BZCY electrolyte was about 10 μm. The anode functional layer (AFL) was overlapped on the anode, but it was difficult to distinguish between the anode and the AFL. The analogous crystallite sizes of the BZCY anode and the AFL from XRD patterns might be suggested to be the reason for the ambiguous boundary of the anode and the AFL.

Fig. 6 indicates the impedance spectra of the tubular BZCY cell. With decreasing the temperature, the Nyquist plots of the BZCY cell moved into a range of the high value. The ohmic resistance (R_{ohm}) of the BZCY cell, especially, showed significant increase as the operating temperature was diminished from 700 °C to 650 °C. The ohmic resistances of the tubular-type BZCY cell as a function of the temperatures were about 0.78, 0.94 and 0.99 Ω cm^2 at 700, 650 and 600 °C, respectively. In addition, each polarization resistances (R_p) of the tubular BZCY cell were 0.035, 0.042and 0.055 Ω cm^2 at the operating temperature of 700, 650, and 600 °C, respectively. Zuo et al. reported that when the BZCY material was applied to a planar SOFC, R_{ohm} and R_p were 0.28 Ω cm^2 and 0.17 Ω cm^2 at 700 °C, respectively [6]. The tubular BZCY cell in our study had higher R_{ohm} at the same temperature. As mentioned in the introduction part, the point that the ohmic losses of the tubular cell typically tends to be higher than that of the planar cell should be considered. R_p of the tubular BZCY cell showed significantly lower polarization resistance of electrodes than that of the planar cell. The increased triple phase boundary sites (TPB) derived from a uniform pore size with approximately 34% porosity may result in the low polarization resistance due to the improvement of catalytic activity. The introduction of vacuum slurry coating method is also considered to play a pivotal role in reducing the polarization resistance due to the enhanced interface between the anode and electrolyte.

Fig. 7 indicates the cell voltage and the power density of the tubular BZCY cell at various operating temperatures. The open circuit voltage (OCV) of the tubular BZCY cell tended to decrease with increasing operating temperature. The open circuit voltage (OCV) of the cell was 1.01 V at 700 °C. The OCV depends on gas permeability and ionic conductivity typically. As compared to the oxygen ionic conducing electrolyte like ceria based materials (about 0.9 V at 600 °C) [16], the OCV of the BZCY cell was significantly improved at the same temperature, indicating that the use of a proton conducting material could be suitable for the tubular solid oxide fuel cells at an intermediate temperature. The power density of the anode-supported tubular BZCY cell was about 0.5 Wcm^{-2} at 700 °C. Liu et al. reported that the planar BZCY-based SOFC had 0.650 Wcm^{-2} at 700 °C [17]. The lower performance of our results may be attributed to higher ohmic resistance. The ohmic resistance of the tubular BZCY cell in our work was about 0.78 Ωcm^2 at 700 °C, but that of the planar BZCY cell was only 0.24 Ωcm^2 at 700 °C, which results in higher ohmic losses of the tubular cells due to the long distance between electrodes of the tube for electrical path. The second reason for the difference in the cell performance may be due to the difference of catalytic activity of the cathode materials. In the case of the tubular YSZ cell with LSM cathode, Zhou et al. reported the maximum power density was 0.35 Wcm^{-2} at 800 °C [18]. In present work of the tubular BZCY cell, the power density at 800 °C was above 0.6 Wcm^{-2} (omitted data for the subject on intermediate temperature), which was higher than that of the tubular YSZ sample at the same temperature. Consequently, it is expected that applying the BZCY materials to the tubular cell has a potential to reduce the operating

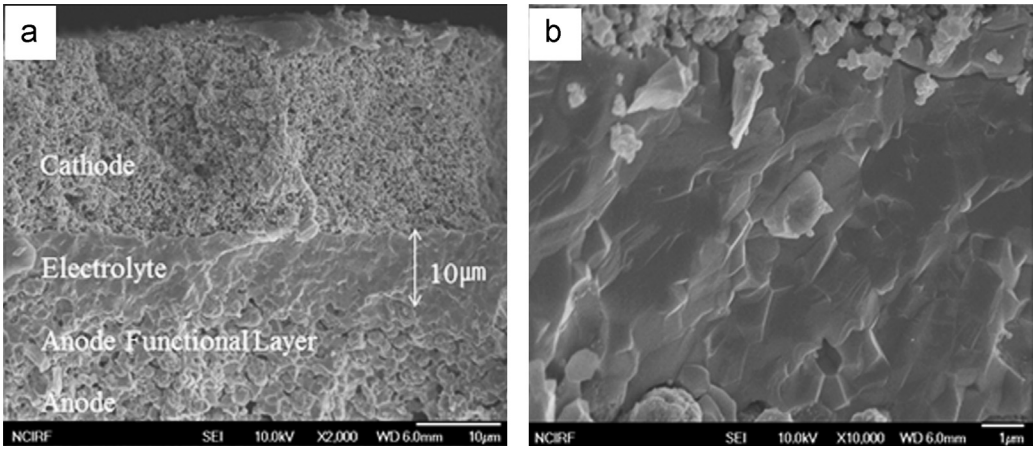

Fig. 5. The cross-sectional SEM morphologies of (a) the tubular-type cell with configuration of Ni–BZCY/AFL/BZCY/LSCF–BZCY and (b) the BZCY electrolyte.

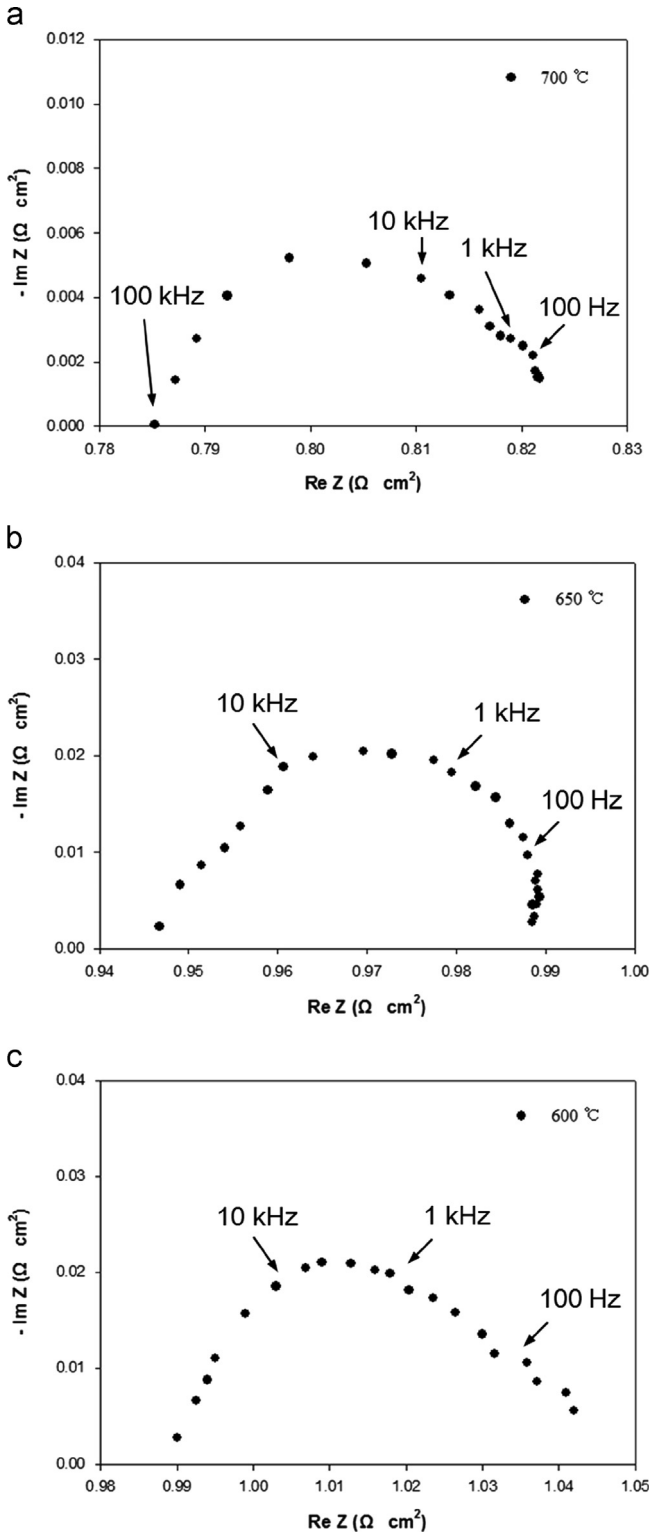

Fig. 6. The impedance spectra of the tubular BZCY cell under open circuit condition depending on operating temperatures: (a) 700 °C, (b) 650 °C, and (c) 600 °C.

temperature of solid oxide fuel cells (SOFCs) and to gain a foothold in a large scale tubular-type cell if further studies such as how to decrease ohmic losses of the tubular cell are performed.

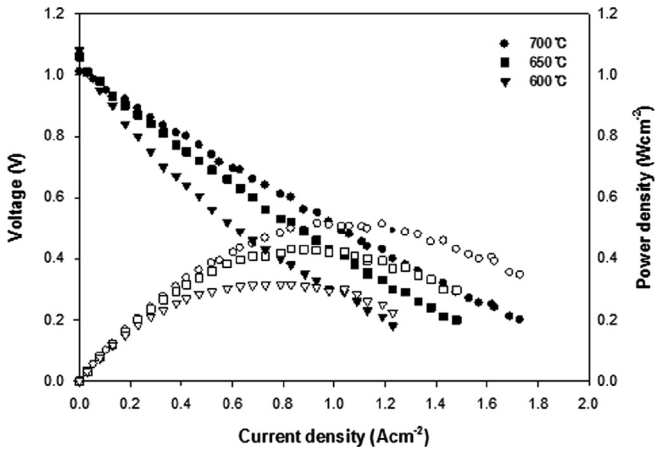

Fig. 7. The cell voltage and the power density of the anode-supported tubular BZCY cell as a function of temperatures.

4. Conclusions

The perovskite-type BZCY materials were successfully applied to the tubular cell as a proton conducting electrolyte. The assembled tubular BZCY cells by each process such as an extrusion and a vacuum assisted dip-coating had well-bonding boundary between the electrodes and the electrolyte. The crystallite sizes of the anode powder and AFL powder synthesized by the wet chemical reaction method were similar, 61.7 nm and 48.5 nm. The ohmic loss and polarization resistance of the tubular BZCY cell were 0.78 and 0.035 Ωcm^2 at 700 °C, respectively. The tubular-type BZCY cell had 1.01 V of the open circuit voltage (OCV) and about 0.5 Wcm^{-1} of the power density at 700 °C.

Acknowledgments

This work was supported by the New & Renewable Energy of the Korea Institute of Energy Technology Evaluation and Planning (KETEP) Grant funded by the Korea government the Ministry of Trade, Industry and Energy, 20113020030010.

References

[1] Ekaterina V. Tsipis, Vladislav V. Kharton, Electrode materials and reaction mechanisms in solid oxide fuel cells: a brief review, Journal of Solid State Electrochemistry 12 (2008) 1367–1391.
[2] Ali Volkan Akkaya, Electrochemical model for performance analysis of a tubular SOFC, International Journal of Energy Research 31 (2007) 79–98.
[3] S.P.S. Badwal, K. Foger, Solid oxide electrolyte fuel cell review, Ceramics International 22 (1996) 257–265.
[4] S.C. Singhal, Solid oxide fuel cells for stationary, mobile, and military applications, Solid State Ionics 152-153 (2002) 405–410.
[5] C. Brahim, A. Ringuede, E. Gourba, M. Cassir, A. Billard, P. Briois, Electrical properties of thin bilayered YSZ/GDC SOFC electrolyte elaborated by sputtering, Journal of Power Sources 156 (2006) 45–49.
[6] Chendong Zuo, Shaowu Zha, Meilin Liu, Masaharu Hatano, Makoto Uchiyama, $Ba(Zr_{0.1}Ce_{0.7}Y_{0.2})O_{3-\delta}$ as an electrolyte for low-temperature solid-oxide fuel cells, Advanced Materials 18 (2006) 3318–3320.

[7] Lei Yang, Ze Liu, Shizhong Wang, YongMan Choi, Chendong Zuo, Meilin Liu, A mixed proton, oxygen ion, and electron conducting cathode for SOFCs based on oxide proton conductors, Journal of Power Sources 195 (2010) 471–474.
[8] Tiago Falcade Celia de Fraga Malfatti, Fuel cell: A Review and a New Approach About YSZ Solid Oxide Electrolyte Deposition Direct on LSM Porous Substrate by Spray Pyrolysis, 2012.
[9] N.M. Sammes, Y. Du, R. Bove, Design and fabrication of a 100 W anode supported micro-tubular SOFC stack, Journal of Power Sources 145 (2005) 428–434.
[10] Jong-Hee Kim, Rak-Hyun Song, Keun-Suk Song, Sang-Hoon Hyun, Dong-Ryul Shin, Harumi Yokokawa, Fabrication and characteristics of anode-supported flat-tube solid oxide fuel cell, Journal of Power Sources 122 (2003) 138–143.
[11] Lan Zhang, Hong Quan He, Wen Rui Kwek, Jan Ma, Ee Ho Tang, San Ping Jiang, Fabrication and Characterization of anode-supported tubular solid-oxide fuel cells by slip casting and dip coating techniques, Journal of the American Ceramic Society 92 (2) (2009) 302–310.
[12] Cengiz Kaya, Stuart Blackburn, Extrusion of ceramic tubes with complex structures of non-uniform curvatures made from nano-powders, Journal of the European Ceramic Society 24 (2004) 3663–3670.
[13] N.M. Sammes, Yanhai Du, Fabrication and characterization of tubular solid oxide fuel cells, International Journal of Applied Ceramic Technology 4 (2) (2007) 89–102.
[14] M. Galceran, M.C. Pujol, M. Aguilo, F. Diaz, Sol–gel modified Pechini method for obtaining nanocrystalline $KRE(WO_4)_2$ (RE=Gd and Yb), Journal of Sol–Gel Science and Technology 42 (2007) 79–88.
[15] Hui-Jeong Son, Rak-Hyun Song, Tak-Hyoung Lim, Seung-Bok Lee, Sung-Hyun Kim, Dong-Ryul Shin, Effect of fabrication parameters on coating properties of tubular solid oxide fuel cell electrolyte prepared by vacuum slurry coating, Journal of Power Sources 195 (2010) 1779–1785.
[16] C. Hatchwell, N.M. Sammes, I.W.M. Brown, Fabrication and properties of $Ce_{0.8}Gd_{0.2}O_{1.9}$ electrolyte-based tubular solid oxide fuel cells, Solid State Ionics 126 (1999) 201–208.
[17] Mingfei Liu, Jianfeng Gao, Xingqin Liu, Guangyao Meng, High performance of anode supported $BaZr_{0.1}Ce_{0.7}Y_{0.2}O_{3-\delta}$ (BZCY) electrolyte cell for IT-SOFC, International Journal of Hydrogen Energy 36 (2011) 13741–13745.
[18] Liu Zhou, Mojie Cheng, Baolian Yi, Yonglai Dong, You Cong, Weishen Yang, Performance of an anode-supported tubular solid oxide fuel cell (SOFC) under pressurized conditions, Electrochimica Acta 53 (2008) 5195–5198.